ARCHIVES OF ELECTRICAL ENGINEERING VOL. 73(4), pp. 891 –906 (2024)

DOI 10.24425/aee.2024.152101

Research on the impact of inter-turn short circuit faults on the electromagnetic and thermal characteristics of closed oil-cooled back-wound high-speed permanent magnet generator

XUANDONG WU[1], JIANAN LU[2], MINGMING CAO[2]✉, HONGBO QIU[2]

[1] *Wolong Electric Nanyang Explosion-proof Group*
Nanyang city, Henan, China

[2] *School of Electric and Information Engineering, Zhengzhou University of Light Industry*
Zhengzhou city, No. 5 Dongfeng Road, Henan, China

e-mail: 2280356740@qq.com, {wy11977/✉cmm03203604}@163.com

(Received: 06.03.2024, revised: 12.11.2024)

Abstract: The oil-cooled back-wound high-speed permanent magnet generator (OBHPMG), is suitable for the aerospace field, gas turbines, and flywheel energy storage due to its high efficiency as well as high-power density. However, the high-power density operation of the generator inevitably results in a significant temperature rise, particularly when inter-turn short circuit faults (ISCFs) occur in the windings. In order to clarify the electromagnetic as well as thermal characteristics of the OBHPMG under the different ISCF degrees, it is of great significance to research the electromagnetic and temperature field variation characteristics of the generator at various inter-turn short circuit faults degrees. Firstly, the electromagnetic field of the 40 kW OBHPMG is investigated at normal operating in this paper, the rotor eddy current densities as well as stator core magnetic flux densities distribution is determined. Secondly, based on the model of the generator ISCF, the effects of the winding different ISCF degrees on the rotor eddy current densities and stator core magnetic flux densities are further explored in detail. The variation characteristics of the rotor current loss as well as stator core magnetic flux densities under the winding different ISCF degrees are revealed. Finally, the effect of the different ISCF degrees on the windings and permanent magnets temperature is analyzed in depth by combining the variation mechanism of the electromagnetic loss. The temperature variation characteristics of the OBHPMG with the different ISCF degrees are obtained, and the cooling effect of the OBHPMG under the ISCF is clarified. It provides a theoretical basis for clearly mastering the variations in the performance of the generator under the windings ISCF in this paper.

Key words: closed oil-cooled back-wound high-speed permanent magnet generator, cooling effect, electromagnetic as well as thermal characteristics, inter-turn short circuit faults

© 2024. The Author(s). This is an open-access article distributed under the terms of the Creative Commons Attribution-NonCommercial-NoDerivatives License (CC BY-NC-ND 4.0, https://creativecommons.org/licenses/by-nc-nd/4.0/), which permits use, distribution, and reproduction in any medium, provided that the Article is properly cited, the use is non-commercial, and no modifications or adaptations are made.

www.czasopisma.pan.pl PAN POLSKA AKADEMIA NAUK www.journals.pan.pl

1. Introduction

In recent years, the high-speed permanent magnet generator has been widely used in the fields of military, medical treatment and mine rescue [1]. As the core equipment of the power generation system, there are a number of significant advantages of the high-speed permanent generator, such as small size, high-speed, high-power density and so on [2–4]. However, the losses increase dramatically with the generator operating in high speed, which results the generator temperature rise is too high. Especially the generator electromagnetic as well as temperature field vary significantly when the windings inter-turn short circuited, which seriously affects the operating efficiency of the generator and shortens its service life [5–7]. Meanwhile, accurately mastering the electromagnetic as well as thermal characteristics of the OBHPMG at different ISCF degrees is the basis to keep the generator operating stably and prolong its operating life. Therefore, it is necessary to investigate the electromagnetic as well as temperature field variation characteristics of the generator at different ISCF degrees.

The electromagnetic or temperature field of the generator under conventional cooling methods has been extensively investigated and analyzed nationally and internationally. Xinggang Fan *et al*. [8] investigated the ventilation and thermal performance of radial forced-air-cooled fractional slot concentrated winding (FSCW) permanent magnet synchronous wind generator (PMSWG). A new ventilation structure was proposed, and its impact on temperature and flow distribution was analyzed using the computational fluid dynamics (CFD) method. The results showed that the new structure could enhance heat dissipation. Kevin Bersch *et al*. [9] proposes a synchronous generator optimization method combining thermal and electromagnetic. This optimization method is applied to optimize the stator ventilation holes of a motor. The research results indicate that the optimized motor windings exhibit reduced maximum temperature and average temperature. Yanping Liang *et al*. [10] studied the influence of transposition angle on 3-D domain magnetic field of stator bars in water-cooled turbo-generators. They confirmed that the transposition angle of stator bars can affect the uniformity of magnetic-filed distribution in the slot. In addition, some research on generator cooling is studied in other literature [11–13].

The motor is subjected to environmental influences such as mechanical vibration and moisture during operation. Due to the high-power density of high-speed motors, the temperature rise of the generator is relatively high. If the motor operates under these conditions for a long time, it is prone to damage the insulation of the stator winding, leading to short circuits between turns [14, 15]. Sun Z.G. *et al*. [16] used analytical methods and finite element methods to calculate the changes in self-inductance, mutual inductance, and inter-turn short-circuit currents of the faulty phase windings under different short-circuit positions. P. Arumugam *et al*. [17] proposed a vertical distributed winding structure and conducted analytical calculations on the inter-turn short-circuit characteristics of the motor based on the distribution of magnetic field lines inside the slots under this structure. Based on monitoring changes in three-phase line currents and phase voltages, Monia Ben Khader Bouzid *et al*. [18] proposed a neural network method for automatic detection and localization of inter-turn short-circuit faults in induction motor stator windings.

There are very few reports on the electromagnetic as well as temperature field variation features of the oil-cooled back-wound high-speed permanent magnet generator (OBHPMG) under the windings ISCF. In this paper, based on the electromagnetics mechanics as well as heat transfer theory, the 40 kW OBHPMG is regarded as the research object. Firstly, through investigating the

electromagnetic field of the generator at high-speed operating, the rotor eddy current densities and stator core magnetic flux densities distribution is determined. Secondly, through researching the effects of the winding different ISCF degrees on the rotor eddy current densities and stator core magnetic flux densities in detail, the variation characteristics of the rotor current loss as well as stator core magnetic flux densities under the winding different ISCF turns are revealed. Finally, the temperature variation characteristics of the OBHPMG with the different short circuit turns are obtained by analyzing the effect of the different ISCF degrees on the windings and permanent magnets and combining the variation mechanism of the electromagnetic loss. In addition, the accuracy of the research analysis is demonstrated by comparing the mathematical calculations with the electromagnetic and temperature rise experimental results. It provides a theoretical basis for clearly mastering the variations in the performance of the generator under the windings inter-turn short circuit in this paper.

2. Description of OBHPMG ISCF model

2.1. Closed oil cooling system of BHPMG

In order to achieve stable and reliable operation of the generator at high speed, a new closed oil cooling structure aimed at the BHPMG is proposed. In the closed oil cooling structure, the oil duct includes the back oil duct flowing through the back winding as well as the internal oil duct flowing through the stator slot winding, and the oil duct exists only outside the oil baffle ring. When the OBHPMG is in high-speed operation, the cooling oil flows into the oil inlet on the lower right, flowing through the oil recess on the generator right side. It flows through the back windings and stator windings, and enters into the back oil duct and internal oil duct. After cooling the generator, the cooling oil flows out the oil outlet on the upper left. The closed oil cooling system of the BHPMG is illustrated in Fig. 1.

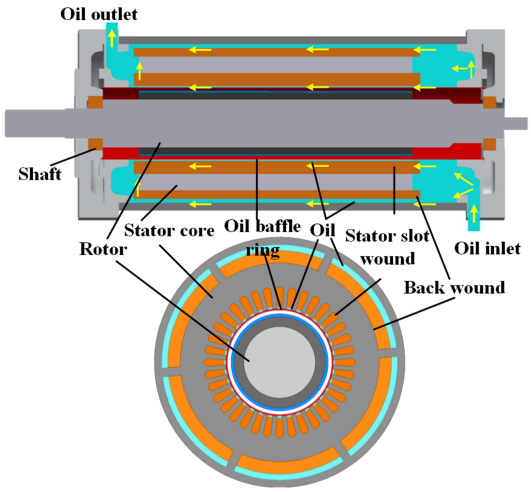

Fig. 1. Closed oil cooling system of the BHPMG

2.2. The model of OBHPMG ISCF

The electromagnetic as well as temperature field distributions of the OBHPMG at inter-turn short circuit faults vary significantly, especially there are obvious differences in the electromagnetic as well as temperature field distribution as the generator short circuit faults degrees increase. In order to deeply analyze the variation characteristics of the electromagnetic as well as temperature field of the generator at different ISCF degrees, the model of the OBHPMG ISCF is established, as shown in Fig. 2. And the basic parameters of the OBHPMG as shown in Table 1.

Table 1. The OBHPMG basic parameters

Parameters (unit)	Value	Parameters (unit)	Value
Number of turns per slot	5	Frequency (Hz)	333.33
Pole number	2	Stator outer diameter (mm)	135
Rotor type	PM	Stator inner diameter (mm)	73
Rated speed (rpm)	20 000	Rotor outer diameter (mm)	66
Slot number	36	Stator length (mm)	275

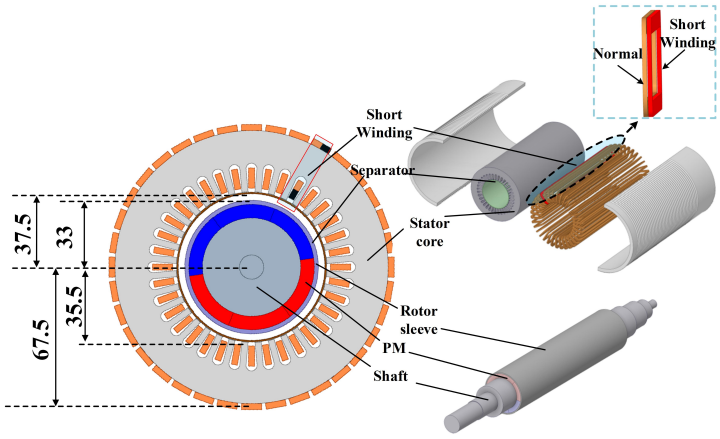

Fig. 2. The model of the OBHPMG ISCF

2.3. Description of OBHPMG global fluid-heat transfer coupling model

The oil movement inside the back oil duct and internal oil duct is very complicated especially the generator is inter-turn short circuited. The fluid in the generator should be satisfied the basic physical conservation laws, including the law of energy conservation, the law of momentum conservation, as well as the law of mass conservation [19].

www.czasopisma.pan.pl PAN POLSKA AKADEMIA NAUK www.journals.pan.pl

Energy conservation equation:

$$\frac{\partial(\rho u)}{\partial x} + \frac{\partial(\rho v)}{\partial y} + \frac{\partial(\rho w)}{\partial z} = 0. \tag{1}$$

Momentum conservation and mass conservation equation:

$$\left\{ \begin{array}{l} \dfrac{\partial(\rho u)}{\partial t} + \operatorname{div}(\rho \boldsymbol{V} u) = \operatorname{div}(\mu \cdot \operatorname{grad} u) - \dfrac{\partial p}{\partial x} + S_u \\ \dfrac{\partial(\rho v)}{\partial t} + \operatorname{div}(\rho \boldsymbol{V} v) = \operatorname{div}(\mu \cdot \operatorname{grad} uv) - \dfrac{\partial p}{\partial y} + S_v \\ \dfrac{\partial(\rho w)}{\partial t} + \operatorname{div}(\rho \boldsymbol{V} w) = \operatorname{div}(\mu \cdot \operatorname{grad} w) - \dfrac{\partial p}{\partial y} + S_w \\ \dfrac{\partial \rho}{\partial t} + \operatorname{div}(\rho \boldsymbol{V}) = 0 \end{array} \right\}, \tag{2}$$

where: ρ is the fluid density (kg/m^3), μ is the dynamic viscosity, $\boldsymbol{V}$ is the velocity vector (m/s), u, v, as well as w are the components of $\boldsymbol{V}$ in the x-axis, y-axis, as well as z-axis directions, P is the static pressure on the fluid microelement (Pa), S_u, S_v as well as S_w are the source items of the momentum equation.

In addition, the internal oil flowing of the generator is in turbulent state, as well as the k-ωSST model [20–22] is used to calculate the complex turbulence in the fluid field. The k-ωSST model is written as:

$$k_w^+ = \max\left\{0, \frac{1}{\sqrt{\beta}} \tanh\left[\left(\frac{\ln\dfrac{h_s^+}{30}}{\ln 10} + 1 - \tanh\frac{h_s^+}{125}\right)\tanh\frac{h_s^+}{125}\right]\right\}, \tag{3}$$

$$w_w^+ = \frac{300}{h_s^{+2}}\left(\tanh\frac{15}{4h_s^+}\right)^{-1} + \frac{191}{h_s^+}\left[1 - e^{\left(-\frac{h_s^+}{250}\right)}\right], \tag{4}$$

$$y^+ = \frac{\rho u_\tau d_w}{\mu}, \tag{5}$$

$$h_s^+ = \frac{\rho u_\tau h_s}{\mu}. \tag{6}$$

For applications, these values are made dimensional using the following relations:

$$k_w = f_w\left(u_\tau, k_w^+\right) = k_w^+ u_\tau^2, \tag{7}$$

$$w_w = f_w\left(u_\tau, w_w^+\right) = \frac{\rho w_w^+ u_\tau^2}{\mu}, \tag{8}$$

where: k_w, w_w are the boundary conditions, y^+ is the non-dimensional variables, h_s^+ is the wall roughness height, and u_τ is the friction velocity.

www.czasopisma.pan.pl PAN POLSKA AKADEMIA NAUK www.journals.pan.pl

3. Electromagnetic field analysis of OBHPMG at the different ISCF degrees

3.1. Impact of different ISCF degrees on the rotor eddy current loss of OBHPMG

When the ISCF occurs in the stator winding, the generator internal magnetic density shows an asymmetric distribution under the short-circuit loop current, which causes variations in generator losses. Meanwhile, the rotor eddy current losses vary significantly as the short-circuit fault degrees increase. Therefore, it is necessary to analyze the rotor eddy current losses of the OBHPMG at different short-circuit fault degrees.

The rotor eddy current losses are calculated as follows [23]:

$$P_e = \frac{1}{T_e} \int_{T_e} \sum_{i=1}^{k} J_e^2 \Delta_e \sigma_r^{-1} l_t \, \mathrm{d}t, \tag{9}$$

where: J_e is the eddy current area unit current density, Δ_e is the unit area, σ_r is the conductivity of the rotor eddy current, l_t is the rotor axial length, as well as P_e is the current loss.

The eddy current electric density distribution of the OBHPMG at different numbers of short-circuit turns is shown in Fig. 3.

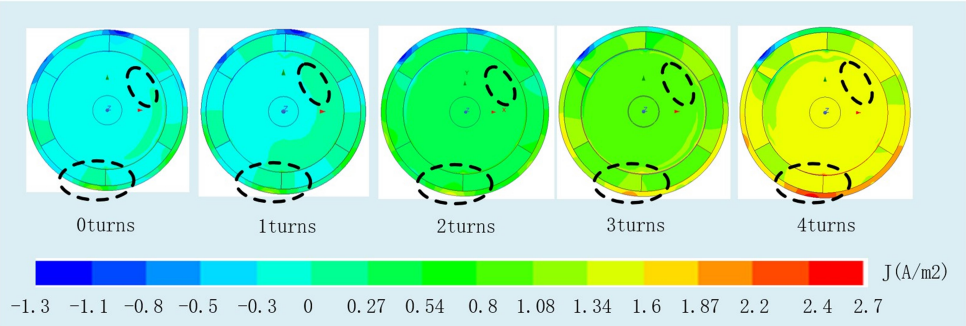

Fig. 3. The OBHPMG eddy current electric density distribution

From Fig. 3, it can be observed that during normal operation of the OBHPMG, the rotor eddy current density is primarily concentrated on the rotor sleeve and the permanent magnets. However, when the ISCF occur in the generator, the short circuit loop current gradually increases with the ISCF degree increase. The air gap magnetic flux density gradually increases, and magnetic flux density distribution gradually shifts, which further accelerates the asymmetric distribution of the air-gap magnetic density. Therefore, the rotor eddy current densities gradually increase with the gradual increase in the number of short circuits, as depicted in Fig. 3. The eddy current density is already distributed throughout the entire rotor when there is a short circuit of 2 turns windings, and the rotor eddy current density increases dramatically when there is a short circuit of 4 turns windings. The maximum eddy current density occurs inside the rotor sleeve.

From the above analysis, the rotor eddy current density gradually increases with the degree of inter-turn short circuit faults (ISCFs) in the windings. Especially, the rotor eddy current density increases sharply when there is a short circuit of 4 turns windings, and the rotor eddy current losses

www.czasopisma.pan.pl PAN POLSKA AKADEMIA NAUK www.journals.pan.pl

are relatively high. In order to further analyze the effect of the short circuit fault degrees on the rotor eddy current losses, the variation characteristics of the rotor eddy current losses as the different windings short circuit turns and contact resistance. These characteristics are illustrated in Fig. 4.

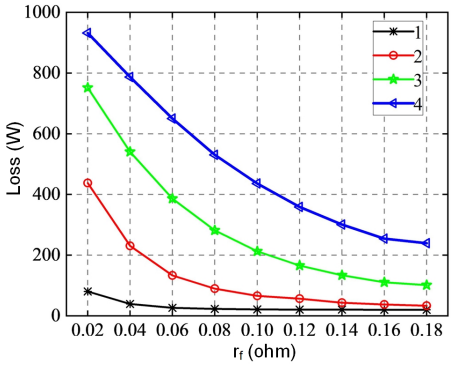

Fig. 4. The variation characteristics of the rotor eddy current losses

Through the above analysis, the rotor eddy current density gradually increases with the windings short circuit turns increase when the contact resistance (rf) remains the same. Therefore, it can be seen from Fig. 4 that under the winding ISCF armature reaction, the rotor eddy current losses increase with windings short circuit turns increase, showing a non-linear variation characteristic. As the windings short circuit turns increase respectively from 1 turn to 2 turns, 2 turns to 3 turns, and 3 turns to 4 turns, the rotor eddy current losses increase respectively from 20.5 W to 37.7 W, 37.7 W to 110.5 W, and 1105 W to 254.2 W, increasing respectively by 1.8 times, 2.9 times, and 2.3 times.

In addition, the rotor eddy current losses decrease with the contact resistance (rf) increase when the number of the windings short circuit turns to keep the same, showing a non-linear variation characteristic. When the windings short circuit turns are respectively 1 turn, 2 turns, 3 turns and 4 turns, as the contact resistance (rf) increase from 0.02 Ω to 0.18 Ω, the rotor eddy current losses respectively decrease from 80.8 W, 437.7 W, 752 W, 932.4 W to 20.2 W, 33.7 W, 101.5 W, 239.7 W, decreasing by 75%, 92.3%, 86.5%, 74.3%. Through the above analysis, it can be shown that the impact of the windings short circuit turns as well as contact resistance (rf) on the rotor eddy current losses is obvious.

3.2. Impact of different ISCF degrees on the stator magnetic flux density of OBHPMG

According to the above analysis, the rotor eddy current electrical density as well as eddy current losses vary significantly when there is an ISCF of the generator. In order to further research the electromagnetic field variation characteristics under the generator inter-short circuit, it is necessary to analyze stator magnetic flux density distribution when the OBHPMG inter-short circuit faults occur. In addition, there are great variations in the stator magnetic flux density distribution of the different parts under the generator inter-short circuit, especially the differences in stator yoke and teeth magnetic flux density distribution are obvious. Therefore, the stator yoke and teeth magnetic flux density distribution at inter-turn short circuit are respectively analyzed in detail, and the stator yoke magnetic flux density distribution at different ISCF degrees is shown in Fig. 5.

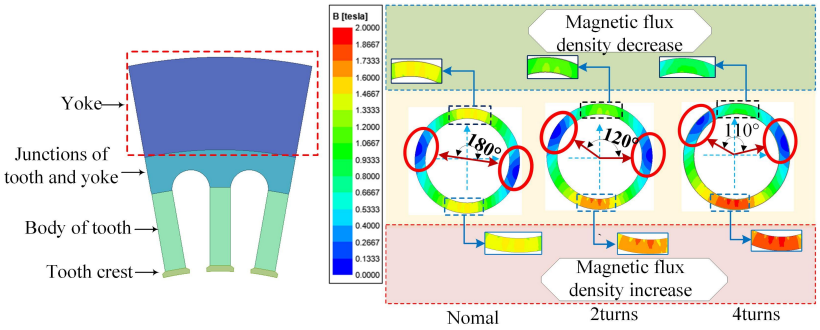

(a) Division of stator core area (b) Magnetic density distribution of stator yoke

Fig. 5. The stator yoke magnetic flux density distribution of the OBHPMG

From Fig. 5, it can be seen that the stator yoke magnetic flux density distribution is uniform as well as symmetric about the origin when the generator operating in normally. The maximum magnetic flux density of the stator yoke is 1.5 T, which is in an unsaturated state. However, the short circuit current is great when the generator is inter-turn short circuited, and the large magnetic field is generated in the stator yoke. The symmetry of the magnetic field is severely disrupted and the magnetic flux density of the stator yoke is no longer symmetrical. Therefore, it can be seen from Fig. 5 that the top magnetic flux density of the stator yoke decrease when the number of the windings short circuit turns is 2 turns, as well as the bottom magnetic flux density increase. The maximum magnetic flux density of the stator yoke reaches 1.8 T, which is in a local saturated state. The magnetic flux density shows a great asymmetric as the number of the windings ISCF turns increases to 4 turns, and the local saturated degrees of the stator yoke increase further. The maximum magnetic flux density of the stator yoke reaches 2 T.

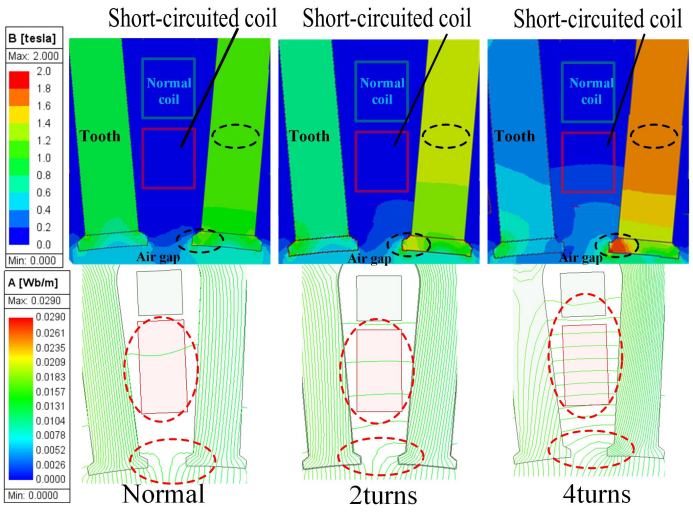

Fig. 6. The stator teeth magnetic flux density distribution of the generator

www.czasopisma.pan.pl PAN POLSKA AKADEMIA NAUK www.journals.pan.pl

According to the above analysis, the saturated degrees of the stator yoke gradually increase as the number of the windings ISCF turns increase, as well as the asymmetric characteristics change obviously. In order to further reveal the variation characteristics of the stator electromagnetic field under generator ISCF, the magnetic flux density and flux lines distribution in the stator teeth were analyzed in detail. The magnetic flux density and flux lines of the stator teeth under different short-circuit degrees are shown in Fig. 6.

From Fig. 6, it can be seen that stator teeth magnetic flux density distribution is uniform as well as it is in an unsaturated state when the generator operates normal. The magnetic flux density of the stator teeth reaches 1.1 T. However, the magnetic density of the stator teeth corresponding to the position of the ISCF slot reaches 1.6 T as the number of the windings ISCF turns increases to 2 turns, increasing by 0.5 T. At the same time, the position of maximum stator magnetic density is transferred from the yoke to the teeth. The saturated degrees of the stator yoke magnetic flux density gradually increases as the number of the windings ISCF turns increases. Especially the magnetic density of the stator teeth corresponding to the position of the ISCF slot reaches 2.1 T as the number of the windings ISCF turns increases to 4 turns. When the generator is in normal operation, the flux lines in the stator teeth are evenly distributed, and only a few magnetic lines enter the stator slot. However, as the number of short-circuit turns increases, the stator teeth gradually saturate, leading to a gradual increase in flux lines through the stator slot, particularly when the short circuit is 4 turns.

4. Temperature field analysis of OBHPMG at the different ISCF degrees

According to the above analysis, it can be seen that the windings current increases rapidly when the ISCF occur in the OBHPMG, as well as the electromagnetic field distribution is not uniform. The generator losses are increased and the temperature rise is too high. In order to clarify the cooling effect of the OBHPMG at ISCF, as well as to clarify the effect of the ISCF degrees on the generator temperature rise, it is necessary to analyze the temperature variation characteristics of the generator at ISCF.

4.1. Effect of the winding ISCF turns on the temperature of the OBHPMG

According to the above analysis, it can be seen that the short circuit current and the degree of the current unbalance gradually increase as the winding short circuit turns increase. Thereby, the harmonics and losses of the generator gradually increase, and the heat generation gradually increases. This will further cause variations in the generator temperature distribution. Therefore, it is necessary to analyze the effect of the winding ISCF turns on the temperature of the generator at ISCF. The temperature distribution of the OBHPMG with the winding ISCF turns of 1 turn as well as 4 turns is shown in Fig. 7.

The losses of the stator back windings are significantly higher than the stator winding when the ISCF occur in the OBHPMG, and the heat generation is particularly concentrated on the back windings. Therefore, it can be seen from Fig. 7 that the generator maximum temperature is distributed on the back windings. And as the number of the winding ISCF turns increases 1 turn to

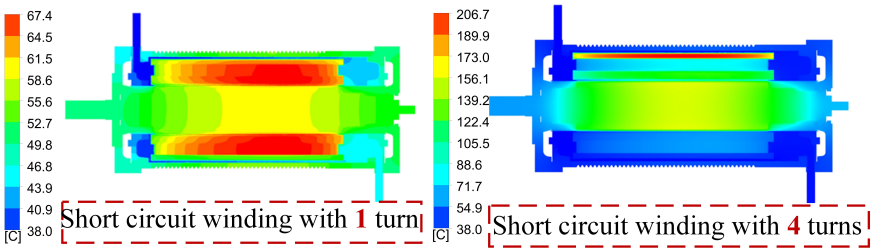

Fig. 7. Temperature distribution of the generator with different ISCF turns

4 turns, it increases from 67.4°C to 206.8°C, increasing by 3.07 times. At the same time, the axial temperature difference of the rotor shaft is greater as the number of the winding ISCF turns increases.

From the above analysis, the OBHPMG temperature rise is low when the winding ISCF turns are 1 turn, as well as the generator can be operated normally under the closed oil cooling system. The OBHPMG not only can operate at high speed, but also it can still run when the generator inter-turn short-circuited. As can be shown the closed oil cooling structure is quite novel and unique.

4.2. Effect of the winding ISCF turns on the windings temperature of the OBHPMG

According to the above analysis, it can be seen that the OBHPMG temperature distribution varies obviously as the number of the winding ISCF turns increases, as well as especially the short circuit windings temperature of the OBHPMG varies significantly. Therefore, it is necessary to analyze the winding temperature field under the different winding ISCF turns in detail. The winding temperature distribution of the generator at short circuit winding turns of 1 turn and 4 turns are shown in Fig. 8.

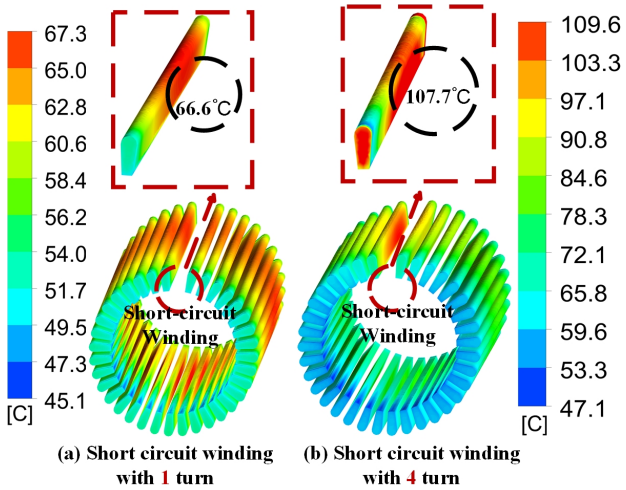

Fig. 8. Stator slot windings temperature distribution with the different winding ISCF turns

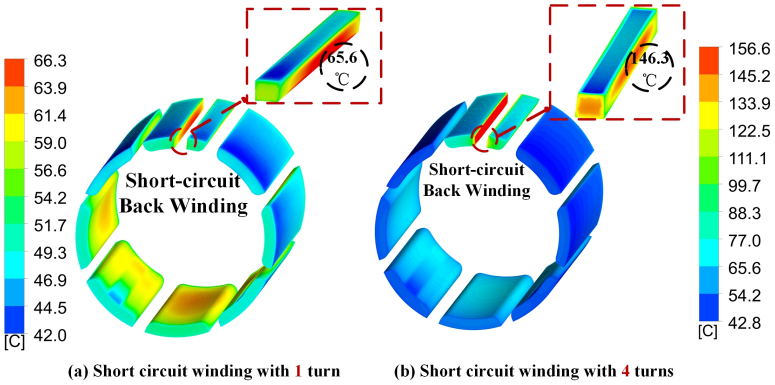

Fig. 9. Back windings temperature distribution with the different short circuit winding turns

According to the stator slot windings temperature distribution analysis in Fig. 8, it can be seen that the blade end temperature of the short circuit windings is higher than other normal windings at the short circuit winding turns of 1 turn and 4 turns due to the heat of short-circuit windings is too concentrated, the short circuit windings maximum temperature reaches respectively 66.6°C and 107.7°C.

In addition, the back windings temperature distribution also varies obviously as the short circuit winding turns increase. In order to further analyze the impact of the winding ISCF turns on the winding temperature of the OBHPMG at ISCF, the back windings temperature distribution with the winding short circuit turns of 1 turn as well as 4 turns is shown in Fig. 9.

From Fig. 9, it can be seen that as the number of the winding ISCF turns increase 1 turn to 4 turns, the back windings maximum temperature increases from 65.6°C to 146.3°C, increasing by 2.2 times. At the same time, the temperature at the end of the short-circuited winding is higher than that at the ends of the other windings.

In addition, as the impact of the heat conduction between the stator as well as the short circuit windings increase when the winding ISCF turns is 1 turn, the temperature of stator and ISCF windings are too high, and the temperature difference between them is small. However, the impact of the heat conduction between the stator and the short circuit windings gradually decreases as the winding short circuit turns increase to 4 turns, the temperature difference between them is great.

4.3. Effect of the winding ISCF turns on the permanent magnet temperature of the OBHPMG

From the above analysis, it can be seen that there is a significant variation in the short circuit windings and permanent magnet temperature distribution with the different winding ISCF turns. At the same time, the performance of permanent magnets is a key factor affecting the operation of the OBHPMG. The permanent magnet temperature distribution of the OBHPMG with the winding short circuit turns of 1 turn and 4 turns is obtained to further clarify the effect of the different winding ISCF turns on the generator temperature. It is shown in Fig. 10.

From Fig. 10, it can be seen that the maximum temperature of the permanent magnets is concentrated in the middle region under the different numbers of the windings short-circuited turns. As the winding short circuit turns increase from 1 turn to 4 turns, the maximum temperature of the permanent magnet increases from 57.8°C to 151.1°C, increasing by 2.6 times.

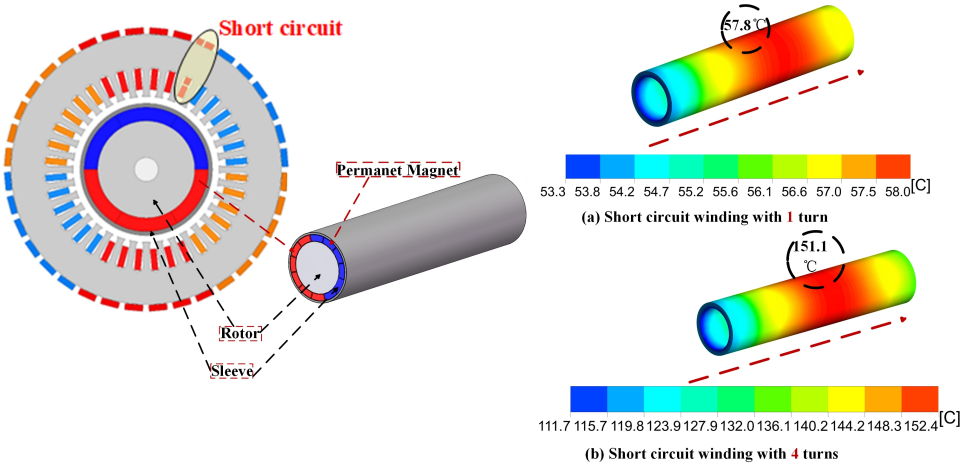

Fig. 10. Permanent magnet temperature distribution with the different ISCF turns

At the same time, as the heat conduction between the rotor shaft and the end bracket gradually increases when the winding short circuit turns increase from 1 turn to 4 turns, the permanent magnet temperature difference along the axial gradually increases. It can be seen that the heat conduction between the rotor shaft and the end bracket is more intense when the temperature is higher.

5. Experimental verification

In order to verify the model analysis accuracy, the experimental platform is built to carry out experiments on the generator electromagnetic performance as well as temperature rise. The experimental equipment mainly includes a drive power supply, two HPMG, a power analyzer, and an oil cooling system. The prototype is equipped with a high-precision temperature sensor to measure the generator internal temperature distribution and a Fluke infrared tester to display the generator external temperature distribution. The experimental platform as shown in Fig. 11.

In the experiment, one HPMG is used as the prime mover to drive another HPMG as the experimental prototype, and the prototype no-load induced electromotive force (EMF) is collected under the rotational speed of 6000 r/min, and the comparison of EMF waveforms obtained from the experiment as well as simulation is shown in Fig. 12.

From Fig. 12, it can be seen that the experimental no-load reverse EMF value is 161.3 V when the generator rotational speed is 6000 r/min, as well as the simulation value is 158.6 V. The difference between the two comparisons is 1.7%, and the waveforms are consistent. As it can be seen that the electromagnetic model analysis is accurate.

The prototype adopts internal and external circulation oil-cooled structure, in which the role of the oil cooler is to provide cooling medium for the motor oil circulation flow. The oil inlet is detected by a flow meter and the inlet flow is controlled by adjusting the flow valve. The temperature measurement system consists of a temperature sensor, an infrared thermal imager and a data acquisition device. In order to accurately measure the temperature inside the motor,

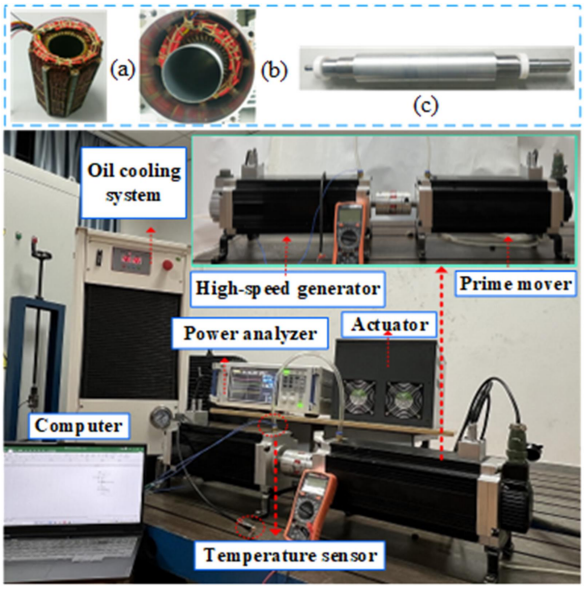

Fig. 11. The experimental platform

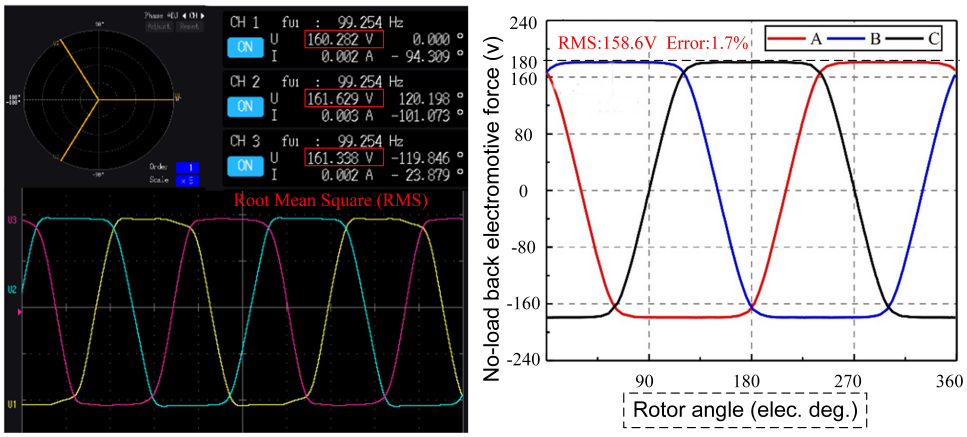

(a) Experimental waveforms (b) Simulation waveforms

Fig. 12. The comparison of EMF waveforms

KTY84-150 temperature sensors were placed. The temperature sensors inside the motor are located on the windings and stator. Measuring the resistance of temperature sensors using a multimeter. The temperature rise of the generator stabilizes after 140 minutes.

Conduct temperature rise experiments on the prototype. In the temperature rise experiment, the prototype surface temperature and at different positions inside the prototype temperature is measured by the Fluke infrared tester and temperature sensor after the prototype temperature rise is stabilized. The experiment test and simulation results are shown in Fig. 13.

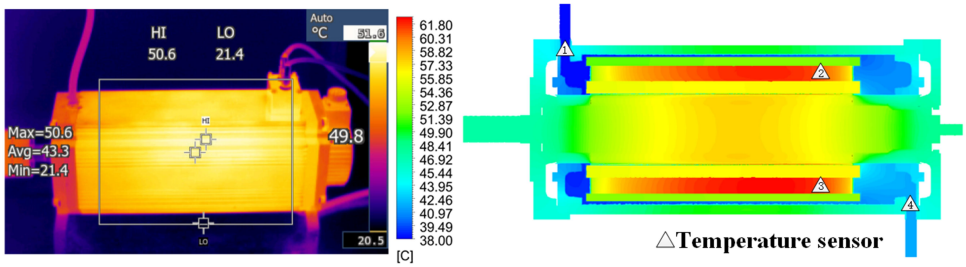

(a) Experimental temperature (b) Simulation temperature

Fig. 13. The comparison of generator temperature

From Fig. 13, it can be seen that experimental prototype surface and winding temperature are respectively 49.8° and 60.3°, and the simulation values are respectively 48.4° and 57.3°. The difference between the two comparisons are respectively 2.9% and 5.2%, and the temperature distribution is consistent. As it can be seen that the temperature model analysis is accurate.

6. Conclusions

In this paper, the 40 kW OBHPMG is regarded as the research object. At the same time, the electromagnetic field of the OBHPMG is investigated, and the effects of different ISCF degrees on the rotor eddy current densities, eddy current losses, and stator core magnetic flux densities are explored. In addition, the temperature variation characteristics of the OBHPMG with the different ISCF degrees are further compared and analyzed by combining the electromagnetic loss variations. More detailed conclusions can be summarised as follows.

1) The rotor eddy current density as well as the rotor eddy current losses both increase with windings ISCF turns increase, showing a non-linear variation characteristic. As the windings ISCF turns increases from 1 turn to 4 turns, the rotor current density increases sharply, as well as the rotor eddy current losses increase from 20.5 W to 254.2 W, increasing by 12.4 times.
2) The asymmetric characteristics of the stator yoke magnetic flux density gradually increase with the degrees of the generator ISCF increase, as well as the saturated degrees of the stator yoke and teeth increase. The magnetic flux density shows a great asymmetric as the number of the windings ISCF turns increases to 4 turns, and the saturated degrees of the stator yoke and teeth both increases. The maximum magnetic flux density of the stator yoke reaches 2 T, as well as the magnetic density of the stator teeth corresponding to the position of the ISCF slot reaches 2.1 T.
3) The OBHPMG temperature gradually increases with the degrees of the genetator ISCF increase, especially the temperatures of the windings and permanent magnet vary most obviously. As the windings ISCF turns increase from 1 turn to 4 turns, the maximum temperature of the stator slot windings, back windings, as well as permanent magnet respectively increase from 66.6°C, 65.6°C, and 57.8°C to 107.7°C, 146.3°C and 151.1°C, increasing by 1.6 times, 2.2 times, and 2.6 times. In addition, the generator under the closed oil cooling can still operate at high speed when the winding is inter-turn short circuited.

www.czasopisma.pan.pl PAN POLSKA AKADEMIA NAUK www.journals.pan.pl

Acknowledgements

This work was supported in part by the Science and Technology Major Program of Henan province under Grant 241100240100, and in part by the National Natural Science Foundation of China under Grant 52177063, and in part by Excellent Young Scholars Project of Henan Province under Grant 232300421070, and in part by the University Science and Technology Innovation Talent Support Program of Henan province under Grant 23HASTIT026, and in part by the Science and technology project of Henan Province under Grant 232102220080, 222102320074, 242102221002.

References

[1] Weili L., Hongbo Q., Xiaochen Z. *et al.*, *Influence of rotor-sleeve electromagnetic characteristics on high-speed permanent magnet generator*, IEEE Transactions on Industrial Electronics, vol. 61, no. 6, pp. 3030–3037 (2013), DOI: 10.1109/TIE.2013.2253074.

[2] Kyung-Hun S., Tae-Kyoung B., Han-Wook C. *et al.*, *Design and analysis of high-speed permanent magnet synchronous generator with rotor structure considering electromechanical characteristics*, IEEE Transactions on Applied Superconductivity, vol. 30, no. 4, 5204305 (2020), DOI: 10.1109/TASC.2020.2980536.

[3] Hong G., Xu H., Jinquan X. *et al.*, *Design of an aviation dual-three-phase high-power high-speed permanent magnet assisted synchronous reluctance starter-generator with antishort-circuit ability*, IEEE Transactions on Power Electronics, vol. 37, no. 10, pp. 12619–12635 (2022), DOI: 10.1109/TPEL.2022.32172339.

[4] Hongbo Q., Yanqi W., Ran Y., *The influence of unbalance load on the electromagnetic and temperature field of high-speed permanent magnet generator*, IEEE Transactions on Magnetics, vol. 55, no. 6, 8200804 (2018), DOI: 10.1109/TMAG.2018.2886434.

[5] Grazia B., Nicola B., *High-speed pm generators for organic Rankine cycle systems: reduction of eddy current rotor losses*, IEEE Transactions on Industry Applications, vol. 55, no. 6, pp. 5800–5808 (2019), DOI: 10.1109/TIA.2019.2935413.

[6] Xiang Z., Tao Y., Serhiy B., *Speed/torque ripple reduction of high-speed permanent magnet starters/generators with low inductance for more electric aircraft applications*, IEEE Transactions on Transportation Electrification, vol. 8, no. 4, pp. 4431–4443 (2022), DOI: 10.1109/TIE.2022.3194972.

[7] Flyur R.I., Luca P., Viacheslav E.V. *et al.*, *Design and performance of a high-speed permanent magnet generator with amorphous alloy magnetic core for aerospace applications*, IEEE Transactions on Industrial Electronics, vol. 67, no. 3, pp. 1750–1758 (2020), DOI: 10.1109/TIE.2019.2905806.

[8] Xinggang F., Ronghai Q., Jian L. *et al.*, *Ventilation and thermal improvement of radial forced air-cooled FSCW permanent magnet synchronous wind generators*, IEEE Transactions on Industry Applications, vol. 53, no. 4, pp. 3447−3456 (2017), DOI: 10.1109/TIA.2017.2686350.

[9] Kevin Bersch, Stefano Nuzzo, Peter H. Connor *et al.*, *Thermal and electromagnetic stator vent design optimization for synchronous generators*, IEEE Transactions on Energy Conversion, vol. 36, no. 1, pp. 207–217 (2020), DOI: 10.1109/TEC.2020.3004393.

[10] Yanping L., Lei W., Xu B. *et al.*, *The influence of transposition angle on 3-D global domain magnetic field of stator bar in water-cooled turbo-generator*, IEEE Transactions on Magnetics, vol. 51, no. 11, 8113804 (2015), DOI: 10.1109/TMAG.2015.2450932.

[11] Shuye D., Xin J., Zhenjiang L. *et al.*, *Research on relativity of flow rate distribution inside the rotor domain for a large-scale air-cooled turbo-generator*, IEEE Access, vol. 7, pp. 174889–174897 (2019), DOI: 10.1109/ACCESS.2019.2943156.

www.czasopisma.pan.pl PAN POLSKA AKADEMIA NAUK www.journals.pan.pl

[12] Byeng D.Y., Kyung M.P., Chao H. *et al.*, *Statistical health reasoning of water-cooled power generator stator bars against moisture absorption*, IEEE Transactions on Energy Conversion, vol. 30, no. 4, pp. 1376–1385 (2015), DOI: 10.1109/TEC.2015.2444873.

[13] Weili L., Jichao H., Xingfu Z. *et al.*, *Calculation of ventilation cooling, three-dimensional electromagnetic fields, and temperature fields of the end region in a large water-hydrogen-hydrogen-cooled turbogenerator*, IEEE Transactions on Industrial Electronics, vol. 60, no. 8, pp. 3007–3015 (2012), DOI: 10.1109/TIE.2012.2202359.

[14] Belguerras L., Mezani S., Gerada C. *et al.*, *Non-linear Circuit Based Model of Permanent Magnet Synchronous Machine Under Inter-turn Fault: a Simple Approach Based on Healthy Machine Data*, IET Electric Power Applications, vol. 7, no. 4, pp. 48–55 (2016), DOI: 10.1049/iet-epa.2015.0443.

[15] Sarikhani A., Mohammed O.A. *et al.*, *Inter Turn Fault Detection in PM Synchronous Machines by Physics-Based Back Electromotive Force Estimation*, IEEE Transactions on Industrial Electronics, vol. 60, no. 8, pp. 3472–3484 (2013), DOI: 10.1109/TIE.2012.2222857.

[16] Sun Z.G., Wang J.B., Howe D. *et al.*, *Analytical prediction of the short-circuit current in fault-tolerant permanent-magnet machines*, IEEE Transactions on Industrial Electronics, vol. 55, no. 12, pp. 4210–4217 (2008), DOI: 10.1109/TIE.2008.2005019.

[17] Arumugam P., Hamiti T., Brunson C. *et al.*, *Analysis of vertical strip wound fault-tolerant permanent magnet synchronous machines*, IEEE Transactions on Industrial Electronics, vol. 61, no. 3, pp. 1158–1168 (2014), DOI: 10.1109/TIE.2013.2259777.

[18] Monia Ben Khader Bouzid, Gérard Champenois, Najiba Mrabet Bellaaj *et al.*, *An effective neural approach for the automatic location of stator inte rturn faults in induction motor*, IEEE Transactions on Industrial Electronics, vol. 55, no. 12, pp. 4277–4289 (2008), DOI: 10.1109/TIE.2008.2004667.

[19] Weili L., Zhaobin C., Xiaochen Z., *Thermal analysis of the solid rotor permanent magnet synchronous motors with air-cooled hybrid ventilation systems*, IEEE Transactions on Industrial Electronics, vol. 69, no. 2, pp. 1146–1156 (2022), DOI: 10.1109/TIE.2021.3057002.

[20] Menter F.R., *Two-equation eddy-viscosity turbulence models for engineering applications*, AIAA Journal, vol. 32, no. 8, pp. 1598–1605 (1994), DOI: 10.2514/3.12149.

[21] Menter F.R., *Zonal two equation k-w turbulence models for aerodynamic flows*, AIAA Journal (1993), DOI: 10.2514/6.1993-2906.

[22] Menter F.R., *Performance of popular turbulence models for attached and separated adverse pressure gradient flows*, AIAA Journal, vol. 30, no. 8, pp. 2066–2072 (1992), DOI: 10.2514/3.11180.

[23] Yunqiu T., Yanping L., *Electric motor electromagnetic field analysis and calculation*, China Machine Press, Beijing, China, pp. 91–93 (2010).